Role of Baroclinic Instability in the Development of Monsoon Disturbances

S. K. MISHRA AND P. S. SALVEKAR

Indian Institute of Tropical Meteorology, Pune 411005

(Manuscript received 22 June 1979, in final form 7 September, 1979)

ABSTRACT

A linear baroclinic stability analysis of the zonal wind representing the mean monsoon situation over India is performed by the use of a multi-level quasi-geostrophic numerical model. An initial value approach is chosen to determine the instability characteristics of the wind. The dependency of the growth rate spectrum on the number of levels in the vertical and on the presence of vertical walls is studied. It is shown that 20 levels in the vertical are sufficient to realize the baroclinic instability of the monsoon mean wind.

A shorter unstable wave of wavelength 1500 km and a longer unstable wave of wavelength 4750 km are found to be the most preferred growing waves from the growth rate spectrum. The shorter unstable wave is essentially confined below 500 mb, whereas the longer unstable wave is above 500 mb. It is also shown that the removal of wind shear below (above) the level of the westerly (easterly) jet from the wind profile, shifts the shorter (longer) unstable wave toward higher wavelengths by ~1000 km, with a significant decrease in the growth rates.

The horizontal scale (1500 km), level of nondivergence (900 mb), and level of maximum intensity (825 mb) associated with the shorter unstable wave are in close agreement with the observed values, obtained from a composite monsoon depression. The computed phase velocity of the unstable wave is opposite to the observed westward motion. The computed levels of cold core, warm core and top of the wave are at 900, 800 and 500 mb, respectively, which are ~100 mb lower than the observed levels. The computed phase velocity of the longer unstable wave (-23 m s^{-1}) is found to be very close to the observed value for disturbances along the easterly jet level. The longer unstable wave has a level of nondivergence at 200 mb which is supported from the results of barotropic studies obtained by others.

1. Introduction

In recent years considerable efforts have been made toward a better understanding of two active disturbances in the summer monsoon flow over India, namely, westward propagating low-level monsoon depressions and upper level waves in the vicinity of the easterly jet. The three-dimensional structure and dynamics of individual depressions have been studied by several workers (Rao and Rajamani, 1970; Krishnamurti *et al.*, 1975, 1976; Daggupaty and Sikka, 1977), and a composite structure was made by Godbole (1977). The three-dimensional synoptic and dynamic structure of wave disturbances along the easterly jet is still more or less unknown. The presence of waves on the 200 mb surface has been noted by Krishnamurti (1971) in his observational study.

Many investigations of pure and combined dynamic instability including CISK (conditional instability of second kind) of the monsoonal zonal wind have been reported by several workers (Shukla, 1977, 1978; Keshavamurty *et al.* 1978), in order to explain the existence of monsoon depressions as an *in situ* formation by the various possible instability mechanism. Shukla (1978) studied the combined barotropic-baroclinic-CISK linear stability properties of the mean monsoon zonal wind. Shukla's computed phase velocity and growth rate for the unstable wave of wavelength 2500 km in the absence of boundary-layer Ekman pumping are in reasonably good agreement with the respective observed mean values for monsoon depressions. His study failed to provide a satisfactory explanation for the observed horizontal scale of monsoon depressions. His other conclusion, which is relevant to the present study, is that the dominant mechanism for the growth of monsoon depressions is CISK and barotropic instability plays a secondary role, while the flow is baroclinically stable.

Many observed features associated with the upper level waves along the easterly jet are simulated by Colton (1973) in a nondivergent, semi-spectral barotropic model which includes dissipation and a forcing mechanism for the ultra long waves. He concluded that the unstable synoptic-scale waves are amplified by drawing kinetic energy from the ultra long waves by barotropic processes. Tupaz *et al.* (1978) have explained the existence and some of the observed special features of these waves as from barotropic instability of the zonally varying easterly jet.

From the above discussion one is tempted to conclude that the growth and maintenance of upper

0022-4928/80/020383-12$07.00

level waves associated with the easterly jet is solely due to the barotropic instability process and that of monsoon depressions is primarily by convective heating (CISK), and that baroclinic instability has not contributed to the growth of monsoon disturbances. This negative role of baroclinic instability, of the summer monsoon flow, in our view, has arisen due to the lack of interest in investigating this instability process and this in turn is due to the following reasons:

1) Charney (1963) has shown with the help of scale analysis that the tropical synoptic-scale motions in the absence of convection are quasi-barotropic to a first approximation, which is quite valid close to the equator but not around the latitude (20°N) where most of the monsoon depressions are formed.

2) The observed vertical shear of zonal wind in the monsoon region between the lower and upper troposphere is generally found to be less than is necessary for baroclinic instability as demanded by the two-level quasi-geostrophic model, which is not valid for the general case with more than two levels in the vertical.

The two-level model seems to be sufficient for a linearly varying basic state in the vertical; but it is incapable of realizing fully the effects of a basic state having considerable variations, as in the case of the monsoonal basic state. Hence, it may be concluded that the number of levels required in the vertical are dependent on vertical structure of the basic-state parameters. The more general necessary condition for baroclinic instability can easily be obtained as a special case of the condition, derived by Charney and Stern (1962) for combined baroclinic-barotropic instability. The computations of Krishnamurti *et al.* (1976) and Keshavamurty *et al.* (1978), based on observed monsoon data over India, have shown that the necessary condition is satisfied in the lower and upper troposphere. The authors feel, based on the above reasons, that the baroclinic instability of the monsoonal zonal wind may contribute to the formative growth of the disturbances in spite of negative results obtained so far. Hence, an attempt is made in this paper to show the importance of baroclinic instability by isolating it from all other possible instability mechanisms.

2. System of equations

a. Equations of model

Mak (1975) has shown by nondimensional analysis that, for synoptic-scale motion, the quasi-geostrophic approximation is quite valid around 17.5°N, the region of our interest, because close to this latitude, monsoon depressions exist to the north and upper level waves in the easterly jet to the south. Therefore, we have considered the quasi-geostrophic model as initially obtained by Phillips (1963).

The two governing equations of quasi-geostrophic adiabatic motion can easily be reduced to a single potential vorticity equation as

$$\left(\frac{\partial}{\partial t} + \mathbf{v}_\psi \cdot \nabla\right)\left[\nabla^2\psi + f_0 + \beta y + f_0^2 \frac{\partial}{\partial p}\left(\frac{1}{\sigma}\frac{\partial \psi}{\partial p}\right)\right] = 0, \quad (2.1)$$

where $\mathbf{v}_\psi = \hat{\mathbf{k}} \times \nabla\psi$, ψ is the streamfunction, the static stability σ is a function of p alone, and the Coriolis parameter f_0 and Rossby parameter β are chosen at latitude 17.5°N. We have assumed rigid horizontal walls at the top and bottom of the atmosphere where $\omega = 0$. The vertical boundary conditions obtained by applying the thermodynamic energy equation at the top and bottom are

$$\left(\frac{\partial}{\partial t} + \mathbf{v}_\psi \cdot \nabla\right)\frac{\partial \psi}{\partial p} = 0$$

at

$$p = 0 \quad \text{and} \quad p = p_0(1000 \text{ mb}). \quad (2.2)$$

The linear form of (2.1) as given below is obtained from the usual linearization process by assuming that the flow consists of a basic zonal flow $\bar{U}(p)$ and a perturbation $\psi'(x,y,p,t)$:

$$\left[\nabla^2 + f_0^2 \frac{\partial}{\partial p}\left(\frac{1}{\sigma}\frac{\partial}{\partial p}\right)\right]\frac{\partial \psi'}{\partial t} + \left[\bar{U}\nabla^2 + \beta - f_0^2 \frac{d}{dp}\left(\frac{1}{\sigma}\frac{d\bar{U}}{dp}\right)\right]\frac{\partial \psi'}{\partial x} + f_0^2 \bar{U} \frac{\partial}{\partial p}\left[\frac{1}{\sigma}\frac{\partial}{\partial p}\left(\frac{\partial \psi}{\partial x}\right)\right] = 0. \quad (2.3)$$

The presence of rigid vertical walls at $y = 0$ and $y = D$ implies $v' = 0$ at the walls and the resulting lateral boundary conditions in terms of ψ' are

$$\psi' = 0 \quad \text{at} \quad y = 0 \quad \text{and} \quad D. \quad (2.4)$$

We consider perturbation as a single wave of wavenumber k in the zonal direction. The wave perturbation which satisfies the lateral boundary condition can be expressed as

$$\psi'(x,y,p,t) = \sin ly[\psi_1(p,t) \times \cos kx + \psi_2(p,t) \sin kx], \quad (2.5)$$

where $l = \pi/D$ and D is the distance between the walls chosen as 3000 km.

The final equation as given below for $\psi_1(p,t)$ and $\psi_2(p,t)$ was obtained by substituting (2.5) in (2.3) and equating cosine and sine coefficients separately to zero:

$$\left[(k^2 + l^2) - f_0^2 \frac{\partial}{\partial p}\left(\frac{1}{\sigma}\frac{\partial}{\partial p}\right)\right]\frac{\partial \psi_L}{\partial t}$$
$$= (-1)^{LL}k\left\{\left[-(k^2 + l^2)\bar{U} + \beta - f_0^2 \frac{d}{dp}\left(\frac{1}{\sigma}\frac{d\bar{U}}{dp}\right)\right]\psi_{LL} + f_0^2\bar{U}\frac{\partial}{\partial p}\left(\frac{1}{\sigma}\frac{\partial \psi_{LL}}{\partial p}\right)\right\}, \quad (2.6)$$

where $LL = 3 - L$; $L = 1, 2$.

The vertical boundary conditions for ψ_1 and ψ_2 were obtained by substituting (2.5) in the linearized form of the boundary conditions (2.2) and once again equating the coefficients to zero:

$$\frac{\partial}{\partial p}\left(\frac{\partial \psi_L}{\partial t}\right) = (-1)^{LL}k\left(\frac{d\bar{U}}{dp}\psi_{LL} - \bar{U}\frac{\partial \psi_{LL}}{\partial p}\right)$$

at

$$p = 0 \quad \text{and} \quad p = p_0. \quad (2.6a)$$

The governing equation (2.6) and the vertical boundary conditions (2.6a) complete the initial value problem. The governing equations in the absence of vertical walls can be easily obtained by putting $l = 0$ in (2.6) while the vertical boundary conditions remain unchanged. ω' (vertical velocity) was computed from the linearized thermodynamic energy equation.

b. Equations for growth rate and phase speed of wave

The wave perturbation (2.5) may be written in the form

$$\psi' = -|\psi| \cos(kx - \delta) \sin ly, \quad (2.7)$$

where $|\psi|$ is the amplitude and δ the zonal phase angle (it indicates the position of wave trough), and are given as

$$|\psi| = (\psi_1^2 + \psi_2^2)^{1/2},$$
$$\delta = \tan^{-1}(-\psi_2/-\psi_1).$$

Under the assumption that the wave is growing exponentially, the growth rate ν and the phase velocity c_r are calculated from the expressions

$$\nu = \frac{1}{2}\frac{d}{dt}[\ln(\mathrm{KE})], \quad (2.8)$$

$$c_r = \frac{1}{k}\frac{\partial \delta}{\partial t}, \quad (2.9)$$

where KE is the wave kinetic energy

$$\mathrm{KE} = \frac{k^2}{4g}\int_0^{p_0}(\psi_1^2 + \psi_2^2)dp.$$

It can be easily shown that relations (2.8) and (2.9) are identical to the respective relations obtained by Brown (1969) for the growth rate and the phase velocity.

3. Basic state

During the summer monsoon season of June–August, depressions form around 20°N and 90°E and most of them show the dominating westward component in their horizontal motion. The easterly jet, along which upper level disturbances move westward, is strongest around 12°N and 80°E at 125 mb during the monsoon season. The common representative basic state zonal vertical wind profile for these two types of disturbances was obtained from the area average of July mean wind between 10 and 25°N, and 75 and 95°E. Presented in Fig. 1a with the dotted line is the vertical distribution of the observed basic state zonal wind. The observed wind profile is represented by an analytical function of the form

$$\bar{U}(p) = \frac{u_1 a^2}{(p - p_1)^2 + a^2} - \frac{u_3 b^2}{(p - p_3)^2 + b^2}, \quad (3.1)$$

where p_1 (125 mb) and u_1 (35 m s^{-1}) are the position and magnitude of the upper level easterly jet, respectively, and p_3 (850 mb) and u_3 (12.5 m s^{-1}) are those of lower level westerly maximum. Constants a and b are related to the surface wind (4 m s^{-1}) and the transition level (450 mb) as shown by Mishra (1979). This analytical representation of the wind is very flexible in the sense that it requires only specification of these six parameters associated with the vertical monsoon wind distribution. The computed wind profile from the analytical function is also shown in Fig. 1a. It can be seen on comparing the two profiles that there is closer agreement between them in the lower troposphere than in the upper troposphere. The analytical profile retained the main characteristics of the observed monsoonal zonal wind quite realistically.

The second basic-state parameter required in this study is the profile of inverse static stability which was obtained from observed data around 17.5°N and is shown in Fig. 1b.

4. Numerical model and procedure

Initial value problem (2.6) was solved by numerical integration. To obtain the finite-difference analogue of (2.6), the atmosphere was divided into N equally spaced layers in the vertical, each of thickness $\Delta p(=p_0/N)$ in pressure as shown in Fig. 2. The layers are represented by dotted lines at mid-points of each layer, whereas the interfaces between the layers are denoted by continuous lines and termed levels. The layer-averaged quantities representative

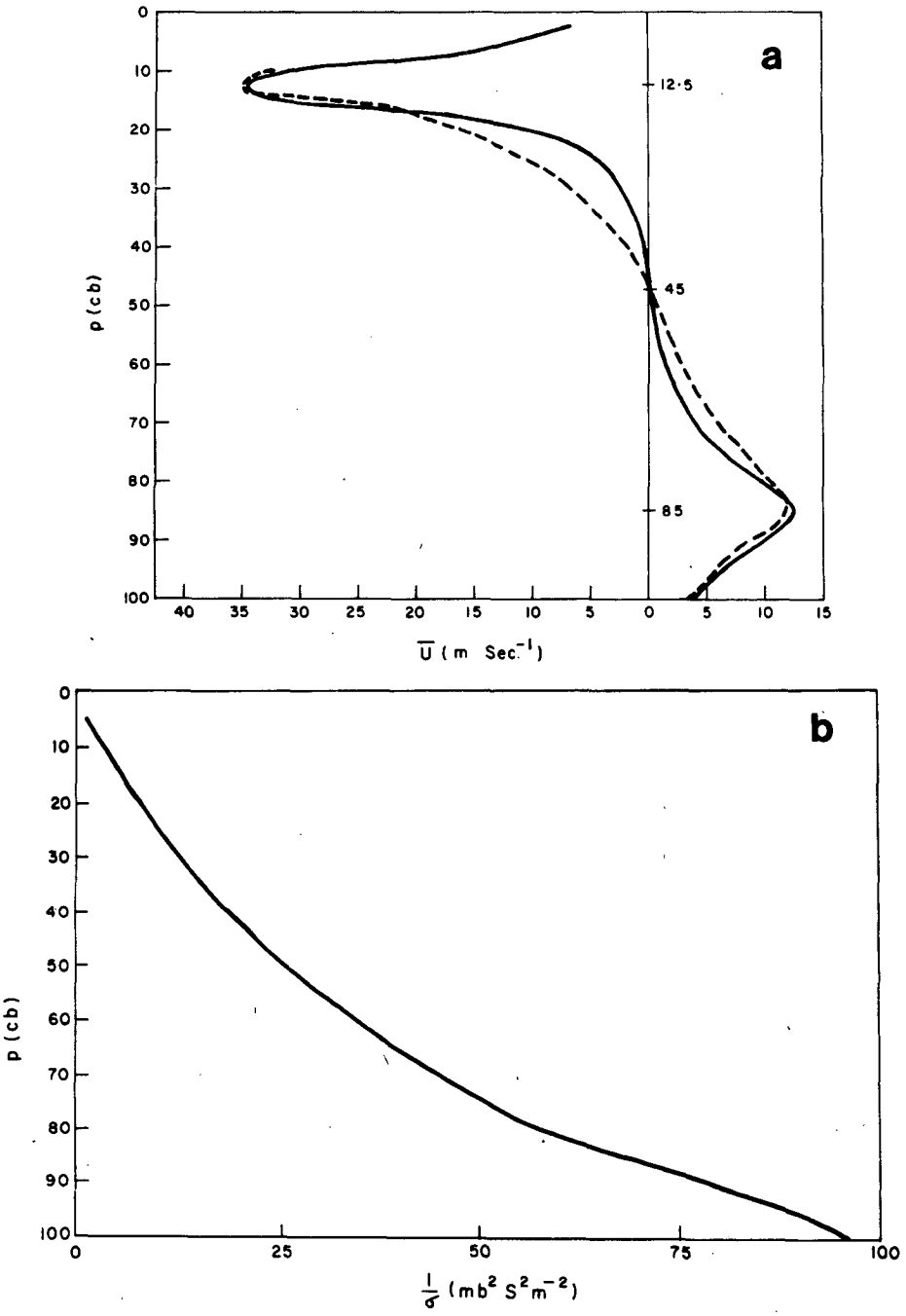

FIG. 1. Vertical profiles of (a) observed mean zonal wind for July (dotted line) and that obtained from Eq. (3.1) (solid line), and (b) observed inverse static stability.

of their values within the layer are shown along the dotted lines. The numerical model equations were obtained after applying Eq. (2.6) at mid-points of each layer and using the centered-difference scheme for the pressure derivatives.

In the equations for the top and bottom layers, the vertical boundary conditions (2.6a) were incorporated with the assumption that the basic zonal flow at the boundaries is equal to the values within the layers, i.e.,

$$\bar{U}_{1/2} = \bar{U}_1 \quad \text{and} \quad \bar{U}_{N+1/2} = \bar{U}_N.$$

It was noted that with this assumption the numerical model discussed here becomes identical to the one derived according to the familiar approach of applying the vorticity equation at the layers and

thermodynamic energy equation at the levels. Further, this assumption does not amount to the additional vertical boundary conditions $d\bar{U}/dp = 0$ at $p = 0$ and $p = 1000$ mb. The partial differential equation (2.6) was reduced to a system of $2N$ coupled ordinary differential equations in $\psi_1(1), \ldots, \psi_1(N)$; $\psi_2(1), \ldots, \psi_2(N)$; which can be written in matrix notation as

$$\mathbf{B}\frac{d}{dt}\begin{bmatrix}\psi_L(1)\\ \psi_L(2)\\ \vdots\\ \psi_L(N)\end{bmatrix} = (-1)^{LL}k\mathbf{A}\begin{bmatrix}\psi_{LL}(1)\\ \psi_{LL}(2)\\ \vdots\\ \psi_{LL}(N)\end{bmatrix}$$

or

$$\frac{d}{dt}\begin{bmatrix}\psi_L(1)\\ \psi_L(2)\\ \vdots\\ \psi_L(N)\end{bmatrix} = (-1)^{LL}k\mathbf{B}^{-1}\mathbf{A}\begin{bmatrix}\psi_{LL}(1)\\ \psi_{LL}(2)\\ \vdots\\ \psi_{LL}(N)\end{bmatrix} \quad . \quad (4.1)$$

Here **A** and **B** are two $N \times N$ matrices, which are functions of basic-state parameters and wavenumber k and l. The explicit form of matrices **A** and **B** are not given here, since they can be easily obtained. For time integration of (4.1), the modified Euler-backward scheme was used for the first time step and for subsequent time steps the leapfrog scheme was used.

At the beginning of each time integration, a baroclinic neutral wave was prescribed by assuming $\psi_2(p,0) = 0$; and by using a suitable profile for $\psi_1(p,0)$, which required a smaller number of time steps to reach the steady state. To determine the appropriate initial profile of $\psi_1(p,0)$, we performed a numerical experiment on dependency of the growth

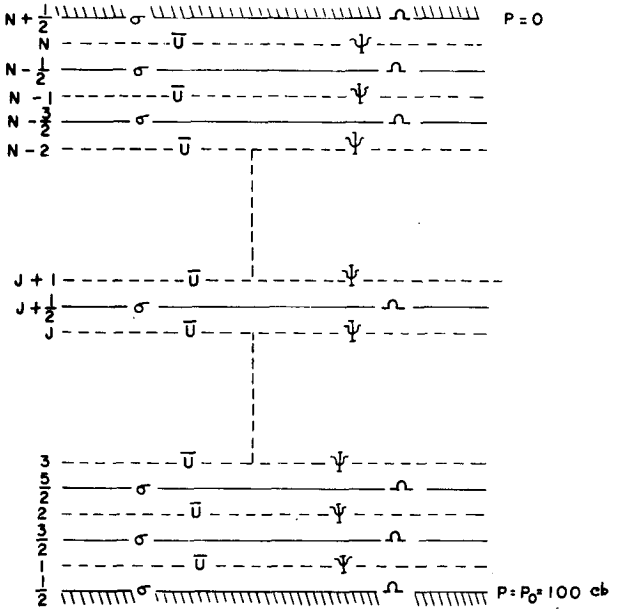

FIG. 2. Schematic diagram of the vertical structure of the N-level model.

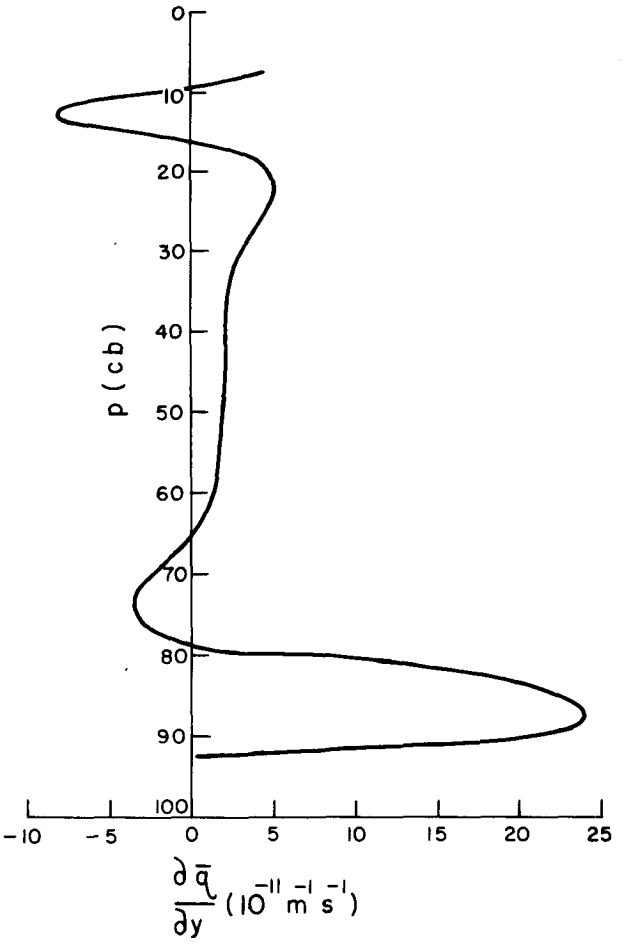

FIG. 3. Vertical profile of the meridional gradient of potential vorticity for 20-level model.

of perturbation on its initial location in the vertical (details are not given here). The results of this experiment show that, in the first few days of time integration, higher growths are noticed if the initial perturbations are in the lower (upper) troposphere for short (long) waves of wavelength smaller (greater) than 3500 km. However, the steady-state growth rate and the structure of the perturbation did not depend on its initial location. Therefore, for the short (long) wavelengths the profiles of $\psi_1(p,0)$ were chosen which remain confined within the lower (upper) troposphere.

The growth rate for each wave was computed from (2.8) at each time step and its 6 h average g_1 was obtained. Similarly, g_2 was designated as the average growth rate for the next 6 h. Then the time integration was continued until the criterion $|(g_1 - g_2)/g_1| < \epsilon$ was satisfied, where $\epsilon = 0.001$.

5. The necessary condition for baroclinic instability

The occurrence of baroclinically unstable waves in the zonal flow $\bar{U}(p)$ is possible, if it satisfies the

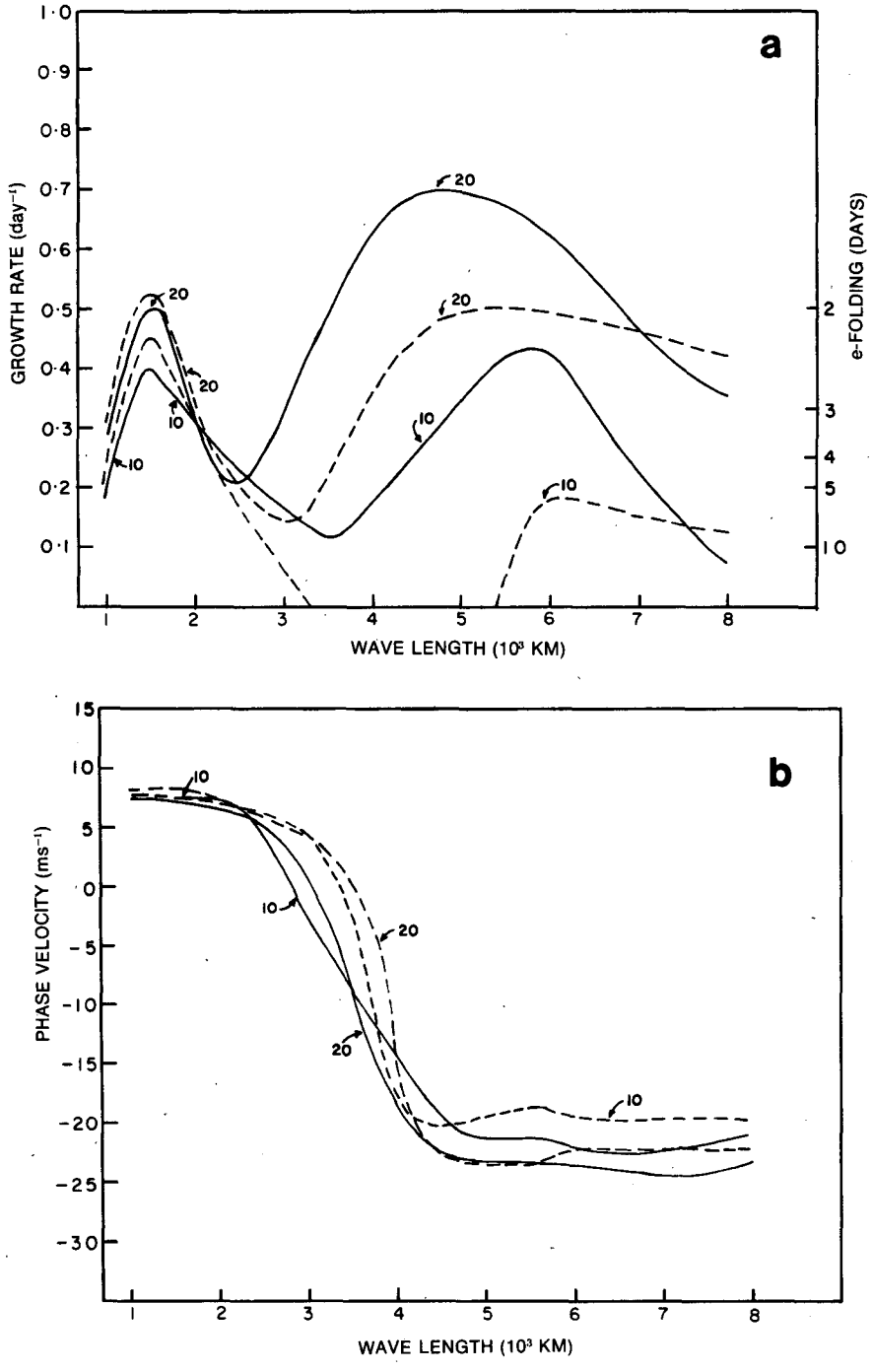

FIG. 4. Dependency of growth rate (a) and phase speed (b) on wavelength and number of vertical levels in the model with (dotted line) and without (solid line) vertical walls.

necessary condition for baroclinic instability (Charney and Stern, 1962). This condition demands that the meridional gradient of potential vorticity

$$\frac{\partial \bar{q}}{\partial y} = \beta - f_0^2 \frac{d}{dp}\left(\frac{1}{\sigma}\frac{d\bar{U}}{dp}\right) \qquad (5.1)$$

must vanish and change its sign somewhere in the vertical domain $[0,p_0]$. The second term in Eq. (5.1) is usually called the baroclinic term. The meridional gradient of basic-state potential vorticity was computed at the various levels for the analytical wind profile and the observed static stability as presented

in Fig. 1. The result of this computation is shown in Fig. 3. It is clear from the profile of $\partial\bar{q}/\partial y$ that the baroclinic instability criterion is satisfied around the four levels—800, 650, 150 and 100 mb. The levels 150 and 100 mb lie below and above the easterly jet level (125 mb) and the level 800 mb is just above the westerly maximum level (850 mb).

6. Growth rate

A range of wavelengths from 1000 to 8000 km at intervals of 500 km was considered for computations in this section. The growth rate and the phase speed for 10- and 20-level models, having no vertical walls, as a function of wavelength are shown in Fig. 4. Comparison between the 20- and 30-level models revealed insignificant differences in growth rate and phase speed. An important point to be noted from the growth rate curves is the presence of two wavelengths of local maximum growth rate, one in the short wavelength region (1000 km $\leq \lambda \leq$ 2500 km) at 1500 km for both the models and the other in the long wavelength region ($\lambda >$ 2500 km) at 4750 and 5500 km for 20- and 10-level models, respectively. It is understood on the basis of instability theory that the wavelength of maximum growth rate corresponds to a possible preferred scale for observed disturbances. It may be concluded here that as a result of baroclinic instability there exists one possible preferred smaller scale near 1500 km and another possible larger scale near 4750 km for disturbances in the monsoon flow. The observed horizontal scale of monsoon depressions as obtained by Godbole (1977) from a composite structure is ~1500 km, and by other workers (Krishnamurti *et al.* 1975; Daggupaty and Sikka, 1977) from individual case studies it is ~2000 km. This is very close to the smaller preferred scale as suggested here. All previous studies on the instability of the monsoon zonal wind show that the baroclinic mechanism has a negative contribution to the growth of perturbations, and this coupled with their failure to provide a satisfactory explanation for the observed horizontal scale of the monsoon depression, lead to the conclusion that only baroclinic instability can possibly provide an explanation for the horizontal scale. The growth rate of the unstable shorter wave is comparable to the value obtained by Shukla (1978), but the phase speed does not agree with observations. The computed unstable wave moves eastward, whereas the mean propagating velocity of monsoon depressions has a westward component.

The preferred larger scale of 4750 km is close to the scale of upper level waves associated with the easterly jet as concluded by Kanamitsu *et al.* (1972) in their observed 200 mb energetics study, by Colton (1973) in his barotropic simulation experiment and by Tupaz *et al.* (1978) in their barotropic instability analysis. The computed growth rate and phase speed of the unstable longer wave is supported by observational evidence and the values obtained by Tupaz *et al.* (1978). They obtained phase speed which is slightly less in comparison to the values obtained here because the easterly jet which they considered had a maximum speed of 30 m s^{-1}, while in the present case this value is 35 m s^{-1}.

a. The growth rate dependency on the number of levels in vertical

The growth rate spectrum (Fig. 4) clearly indicates a general increase in growth rate throughout the range of wavelength with the increase of levels from 10 to 20. This increase is much smaller in the short-wavelength region compared to the long-wavelength region. Further, it may be noted that the wavelength of maximum growth rate in the short-wavelength region remains unchanged, while in the long-wavelength region the maximum is shifted toward shorter wavelengths with the increase in the number of levels. To understand this effect, we computed the average vertical shear of the zonal wind in the lower and upper troposphere for the 10- and 20-level models. On comparison it was noticed that the average wind shear in the upper troposphere for the 20-level model was significantly higher (by ~40%) than the value computed for the 10-level model. No significant difference in the corresponding values for the lower troposphere was found between the two models. As discussed by Staley and Gall (1977), an increase in the wind shear in the upper layers without any change in the lowest layers, increases the zonal available potential energy in the upper layers; this can only be realized by the long waves and not by the small waves because the former have maximum amplitude in the upper layers, while the latter are mostly confined to the lower troposphere. This is why growth rate is expected to increase in the long-wavelength region, but not in the short-wavelength region.

b. The effect of the vertical walls

We will now discuss the effect of the vertical walls on growth rate and phase speed of unstable waves. The computed profiles of growth rate and phase speed obtained from the 10- and 20-level models with vertical walls are presented in Fig. 4 (dotted lines).

The comparison of these results with those obtained in the absence of vertical walls shows no appreciable change in phase velocity throughout the region, but significant changes are noticed in the growth rate spectrum. The growth rates in the short-wavelength region more or less remain unchanged, while they decrease considerably in the long-wave-

length region in the presence of vertical walls. This is consistent with the expectation based on scale analysis that the waves of wavenumber $k \gg l$ are least affected by the presence of walls.

An important feature to be noted in the growth rate spectrum for the 10-level model with the vertical walls is the presence of a gap in a region of wavelengths from 3500 to 5500 km, which was absent for the case without vertical walls. The wave with a length of 3000 km is marginally unstable with a growth rate of <0.1 day^{-1}, while Shukla (1977) has shown that this wave is marginally stable baroclinically in the presence of meridional shear. This discrepancy may be explained by taking into account the effect of meridional shear of the monsoon wind on the baroclinic instability. Brown (1969) has concluded for a westerly jet that the effect of meridional shear on the baroclinic growth rate is similar to the effect introduced by an increase in β. This was expected because in the middle of channel, where the perturbation amplitude was largest, $-\bar{U}_{yy} > 0$ and this resulted in an increase of effective Rossby parameter ($\beta - \bar{U}_{yy}$). In our case the unstable 3000 km wave has the largest amplitude around the level of westerly wind maximum (850 mb) and its amplitude in the upper troposphere is insignificant.

The observed average value of U_{yy}, in our region of interest in the lower troposphere for July, was found to be negative. The effective Rossby parameter is increased due to the meridional shear of the monsoon wind in the lower layers. It was found that the wave of wavelength 3000 km became marginally stable for β corresponding to 10°N. This explains why Shukla (1977) obtained less baroclinically unstable waves in his 10-level model.

c. *The influence of wind shear near the vertical boundaries*

The low-level westerly wind maximum of the monsoon wind lies close to the top of the boundary layer. In this layer non-geostrophic frictional effects dominate over the geostrophic process, which indicates that a major contribution to the vertical shear in the layer below 850 mb (boundary layer) is due to frictional effects. The available potential energy of the basic state within the layer as implied by the quasi-geostrophic approximation is an overestimate to the actual value. It may be quite relevant to know the modifications in the instability characteristics of $\bar{U}(p)$ profile due to the absence of vertical shear within the boundary layer, as an extreme case. For this purpose, the growth rate spectrum (not presented here) was computed for $\bar{U}(p)$ with no vertical shear within the boundary layer, while the wind above this layer was kept unchanged. It was seen from the growth rate curve that there was a considerable decrease of the growth rate in the short-wavelength region, but no significant difference was noticed in the long-wavelength region. Further, it was noted that the decrease in the growth rate was as high as 50% for a wavelength of 1500 km, and the maximum in the short-wavelength region in the growth rate spectrum was shifted toward higher wavelengths close to 2500 km with a value corresponding to an e-folding time of 3.5 days.

A similar computation was carried out with the basic wind having no vertical shear above the level of the easterly jet. The growth rate spectrum computed for this case indicated a maximum decrease of 25% in the growth rate for wavelengths around 5000 km, and no significant difference in the short-wavelength region was noticed; this shifted the growth rate maximum toward longer wavelengths close to 6000 km. The longer unstable wave in this case has an e-folding time of 1.8 days.

7. Structure of the unstable waves

In this section we will discuss the structure of the shorter unstable wave of wavelength 1500 km and that of the longer unstable wave of wavelength 4750 km for the 20-level model without vertical walls. It is obvious from the growth rates that the model without vertical walls requires less integration time to reach a steady state compared to the model with vertical walls. It may be noted that by this choice no further physical reality is lost as evident from following discussion. Either of the lateral boundary conditions considered here does not reflect the true atmospheric situation which is somewhere between the infinite and finite channel in the meridional direction. Differences noticed between the structure of the unstable waves for the model with and without vertical walls are of little consequence.

It is expected that the computed structure of unstable waves obtained here should agree more closely to the observed structure of composite disturbances than that of the individual disturbances. The dominating role of diabatic heating due to condensation in the development of a monsoon depression over land areas has been shown by Krishnamurti *et al.* (1976) with their numerical prediction experiments. Therefore, it is natural to assume that the growth of monsoon depressions by the baroclinic mechanism may be at least a dominating factor in their formative stage over the sea where the upward vertical velocity associated with depression may be small. The vertical velocity field associated with the unstable baroclinic wave may lead to further growth of the depression by wave-CISK. The structure of the depression in the formative stage is not very well known because the formative growth of the depression takes place over the sea. The next alternative is to compare the observed structure of mature monsoon depressions moving across land. Hence,

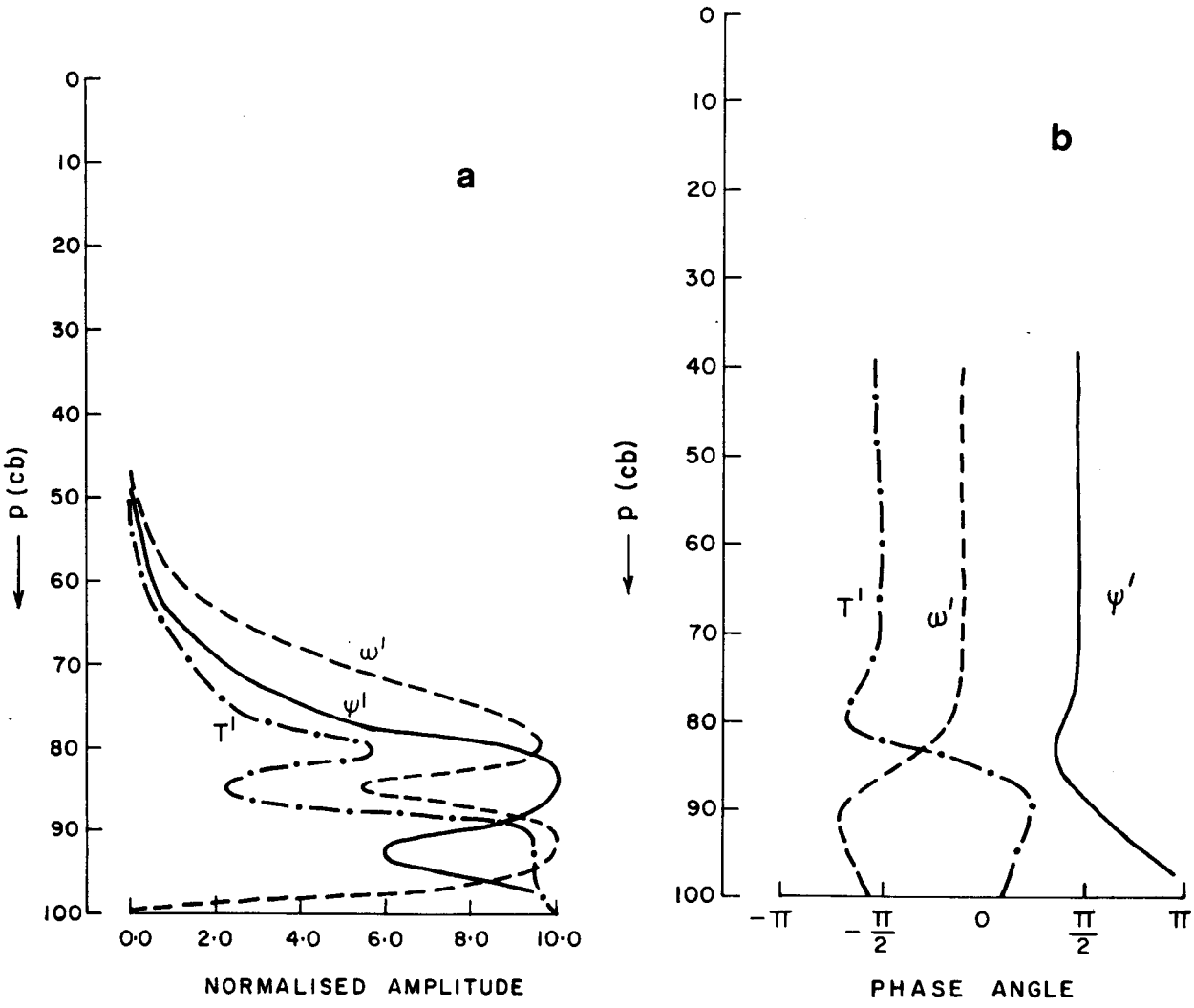

FIG. 5. Vertical structure of amplitude (a) and phase (b) of perturbation streamfunction ($\acute{\psi}+$), vertical velocity ($\acute{\omega}$) and temperature ($\acute{T}$) for the unstable wave of wavelength 1500 km.

the computed structure of the unstable wave of wavelength 1500 km is compared with the structure of the composite monsoon depression as obtained by Godbole (1977). The vertical profile of the amplitude of ψ', ω' and T' are presented in Fig. 5. These profiles indicate that the vertical extension of the wave only reaches 500 mb, whereas the monsoon depression extends at least up to 400 mb. This discrepancy may be due to the neglect of diabatic processes in this study. As shown by the vertical distribution of the amplitude of ψ', the maximum intensity of the wave is at 825 mb level which is quite close to the observed level of 800 mb. The amplitude at the surface is comparable to its maximum value. The surface value may become closer to the observations if the surface friction is included in the model. The vertical profile of the amplitude of vertical velocity shows two maxima at 800 and 900 mb of nearly equal magnitudes and a minimum in between, but the phase angle profile of ω' shows a minimum at the 900 mb level only. Thus, the level 900 mb is the level of nondivergence for the unstable wave. The observed level of nondivergence is near 500 mb as obtained by Godbole using the kinematic method for ω. The level of nondivergence for monsoon depressions as computed by other workers (Krishnamurti *et al.*, 1975; Daggupaty *et al.*, 1978) with the help of a nonlinear ω equation is generally found to be near 850 mb which is close to the level obtained here.

The wave has westward tilt with height in the 1000–850 mb layer and small eastward tilt in the 850–775 mb layer and no vertical tilt further aloft. Observational studies as carried out by various workers on the structure of monsoon depressions failed to indicate any definite vertical tilt. From the

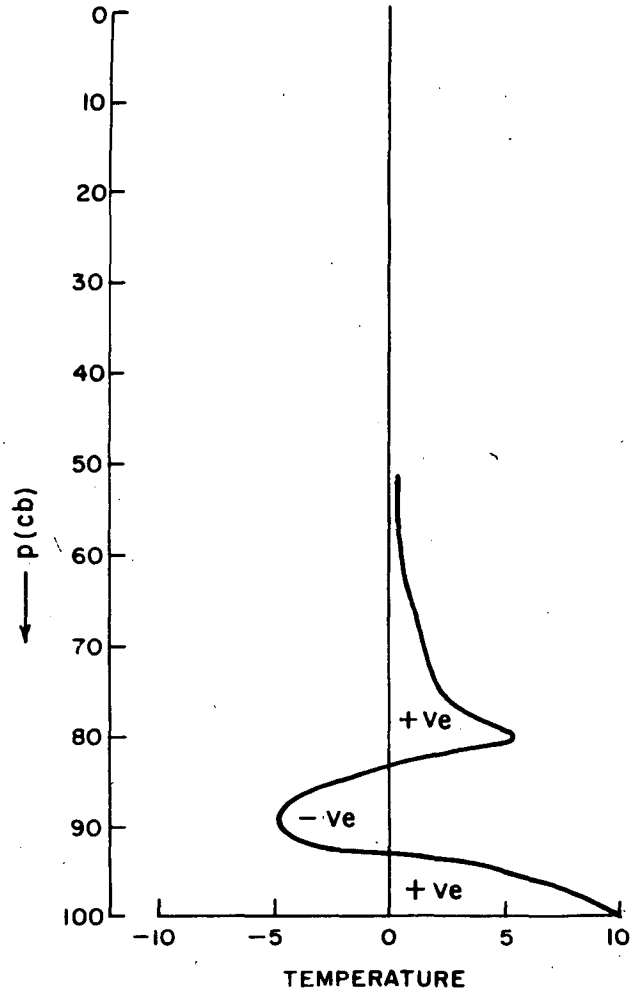

FIG. 6. Vertical distribution of temperature associated with the smaller unstable wave along its trough line (not to scale).

vertical profile of phase of ω', it is clearly seen that maximum upward motion in a horizontal plane takes place to the west of the trough above 900 mb and it is to the east below this level. It may be noted from the vertical profiles of amplitude and phase of ω' presented in Fig. 5 that divergence takes place in the 1000–900 mb layer with convergence in the 900–800 mb layer; further up divergence takes place in the layer above 800 mb. It is clear that the presence of the lowest layer of divergence and the absence of a strong and deep enough middle layer of convergence are responsible for not contributing sufficiently large westward propagation, in order to counteract the eastward propagation due to the advection by the basic-state westerly wind of the lower troposphere; this must eventually result in the westward propagation of the wave.

Fig. 6 shows the computed vertical profile of temperature along the trough of the unstable wave. The profile shows a warm core from the surface to 925 mb and a cold core between 925 mb and 825 mb with maximum intensity at 900 mb and a second warm core above 825 mb with maximum intensity at 800 mb. But the observational study shows a cold core at 800 mb and a warm core at 600 mb. This difference may be due to the fact that the computed wave does not extend sufficiently deep in the vertical; this is why the wave moves in the wrong direction. The surface warm core is generally not observed over land. A surface warming is considered to be favourable for convective activity over the sea. The cold core tilts eastward (Fig. 5) with height up to 900 mb and then westward, while the observed tilt is eastward only.

Fig. 7 shows the vertical distribution of amplitude and phase of ψ', ω' and T' for the unstable longer wave of wavelength 4750 km. The amplitude of ψ' has a maximum at the easterly jet level and very small values in the lower troposphere. This corroborates observational evidence that upper level disturbance in the vicinity of easterly jet is generally not detected in the lower troposphere.

From the phase and amplitude distribution of ω' and ψ', it is clear that vertical upward motion occurs to the west of the trough of ψ' up to 125 mb and downward motion aloft. Vertical upward motion reaches a maximum value at 200 mb and has no tilt around this level, i.e., this corresponds to the level of non-divergence for upper level disturbances. Incidently, this also explains why the phase velocity obtained here agreed so closely with the values obtained by barotropic studies of 200 mb flow as discussed in the previous section. It is expected from theoretical consideration that the steering level of the wave must be above the level of nondivergence, but very close to it. On comparing the $\bar{U}$ profile and the phase velocity, the steering level comes out to be at 170 mb, which is quite close to the level of nondivergence. Convergence of the wave field is to the west of the trough up to 200 mb, and aloft is a layer of divergence up to 50 mb. Convergence is a dominant factor for westward propagation of the wave below 200 mb, while advection and the β effect are dominating factors above this level.

8. Conclusions

The intention in this paper has not been to provide a complete explanation to the problem of development of monsoon depressions and upper level perturbations in the easterly jet, but to bring out the important contribution of the baroclinic instability of the mean monsoon flow to this problem. It has been shown by a linear, quasi-geostrophic, baroclinic stability analysis, using an initial value approach, that the mean monsoonal zonal wind is baroclinically unstable provided sufficient vertical resolution in the numerical model is ensured.

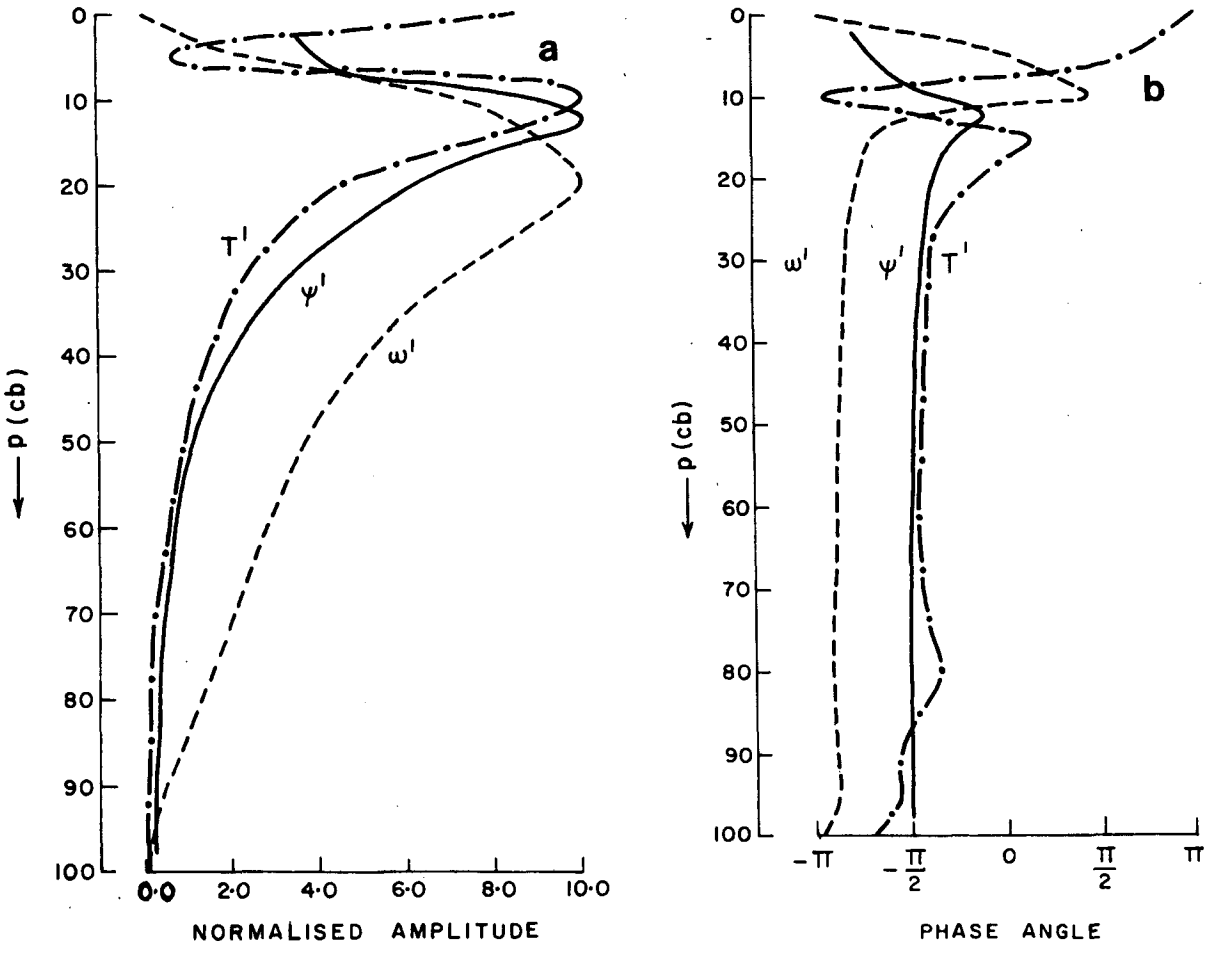

FIG. 7. As in Fig. 5 except for the unstable wave of wavelength 4750 km.

The most interesting and significant result of this study is the presence of two maxima in the growth rate spectrum at wavelengths comparable to the observed horizontal scales of monsoon depressions and the upper level waves. The view that, although the vertical coupling between the tropical upper and lower troposphere over the monsoon region is weak, they are baroclinically active independently, is supported by the results obtained in this paper.

The baroclinic instability mechanism is a primary process for selection of the horizontal scale of disturbances in the lower troposphere. Growth due to baroclinic instability plays an important role, at least in the formative stage of a monsoon depression and in determining its structure. This is evident from the close resemblance shown here, in many aspects, between the computed structure of the shorter unstable wave and the monsoon depression. It is not suggested here that the baroclinic instability mechanism alone is sufficient to evolve monsoon depressions from their formative to mature stages, because the available potential energy of the mean monsoonal flow in the lower troposphere is not sufficient for conversions to potential and kinetic energy associated with observed mature monsoon depressions.

It has been suggested that the baroclinic instability mechanism is also sufficient to explain the existence and development of upper level disturbances in the vicinity of the easterly jet. It has been indicated that their westward motion above the level of nondivergence is mostly controlled by the advection of basic zonal wind and below by convergence associated with the waves.

It has been pointed out that the inviscid, adiabatic and linear baroclinic dynamics of the wave in the zonal wind is not sufficient to explain the westward component of propagation of monsoon depressions. This is consistent with the findings by other workers that westward propagation of monsoon depressions is due to the overriding contribution by strong convergence in the lower layers occuring mostly due to convection, which is not considered here. It seems that to explain the complete northwest propagation of monsoon depressions, further studies

on baroclinic instability of the combined zonal and meridional flow in the presence of convective heating is required.

Acknowledgments. We wish to express our gratitude to Dr. R. Ananthakrishnan for his keen interest, fruitful suggestions and discussions, and are grateful to Dr. D. Subrahmanyam for scientific comments. Thanks are also due to Mrs. S. S. Desai for help in the preparation of the diagrams and to Mrs. V. V. Savant for typing the manuscript. Our sincere thanks to the Director, Dr. Bh. V. Ramana Murty, for continuous support and encouragement. The authors are grateful to an anonymous reviewer for his constructive suggestions and criticism. Computations were carried out on the NCSDCT Dec-10 located at the Tata Institute of Fundamental Research, Bombay, and on the EC-1040 located at the India Meteorological Department, Pune.

One of the authors (P.S.S.) is extremely grateful to Air-India for a research grant.

REFERENCES

Brown, J. A., 1969: A numerical investigation of hydrodynamic instability and energy conversions in the quasi-geostrophic atmosphere. Part I. *J. Atmos. Sci.*, **26**, 352–365.

Charney, J. G., 1963: A note on large scale motions in the tropics. *J. Atmos. Sci.*, **20**, 607–609.

——, and M. E. Stern, 1962: On the stability of internal baroclinic jets in a rotating atmosphere. *J. Atmos. Sci.*, **19**, 159–172.

Colton, D. E., 1973: Barotropic scale interactions in the tropical upper troposphere during the northern summer. *J. Atmos. Sci.*, **30**, 1287–1302.

Daggupaty, S. M., and D. R. Sikka, 1977: On the vorticity budget and vertical velocity distribution associated with the life cycle of a monsoon depression. *J. Atmos. Sci.*, **34**, 773–792.

Godbole, R. V., 1977: The composite structure of the monsoon depression. *Tellus*, **29**, 25–40.

Kanamitsu, M., T. N. Krishnamurti and C. Depradine, 1972: On scale interaction in the tropics during northern summer. *J. Atmos. Sci.*, **29**, 698–706.

Keshavamurthy, R. N., G. C. Asnani, P. V. Pillai and S. K. Das, 1978: Some studies of the growth of monsoon disturbances. *Proc. Indian Acad. Sci.*, **87A**, 61–75.

Krishnamurti, T. N., 1971: Observational study of the tropical upper tropospheric motion field during the northern hemisphere summer. *J. Appl. Meteor.*, **10**, 1066–1096.

——, M. Kanamitsu, R. Godbole, C. B. Chang, F. Carr and J. Chow, 1975: Study of a monsoon depression (I) synoptic structure. *J. Meteor. Soc. Japan*, **53**, 227–239.

——, ——, ——, ——, —— and ——,1976; Study of a monsoon depression (II) dynamical structure. *J. Meteor. Soc., Japan*, **54**, 208–225.

Mak, M. K., 1975: The monsoonal mid-tropospheric cyclogenesis. *J. Atmos. Sci.*, **32**, 2246–2253.

Mishra, S. K., 1979: Some analytical vertical profiles of monsoonal zonal wind over India. *Arch. Meteor. Geophys. Bioklim.*, A (in press).

Phillips, N. A., 1963: Geostrophic motion. *Rev. Geophys.*, **1**, 123–176.

Rao, K. V., and S. Rajamani, 1970: Diagnostic study of a monsoon depression by geostrophic baroclinic model. *Indian J. Meteor. Geophys.*, **21**, 187–194.

Shukla, J., 1977: Barotropic-baroclinic instability of mean zonal wind during summer monsoon. *Pure Appl. Geophys.*, **115**, 1449–1462.

——, 1978: CISK-barotropic-baroclinic instability and the growth of monsoon depressions. *J. Atmos. Sci.*, **35**, 495–508.

Staley, D. O., and R. L. Gall, 1977: On the wavelength of maximum baroclinic instability. *J. Atmos. Sci.*, **34**, 1679–1688.

Tupaz, J. B., R. T. Williams and C. P. Chang, 1978: A numerical study of barotropic instability in a zonally varying easterly jet. *J. Atmos. Sci.*, **35**, 1265–1280.